Reduced order modeling of hysteretic structural response in seismic risk assessment

Dimitrios Patsialis
Graduate Student, Department of Civil and Environmental Engineering and Earth Sciences, University of Notre Dame, Notre Dame, United States

Alexandros A. Taflanidis
Associate Professor, Department of Civil and Environmental Engineering and Earth Sciences, University of Notre Dame, Notre Dame, United States

ABSTRACT: Modern seismic risk/loss estimation practices require simulation of structural behavior for different levels of earthquake shaking through time-history analysis. This behavior can be strongly inelastic/hysteretic and evaluating it through high-fidelity finite element models introduces a significant computational burden. A reduced order modeling approach is discussed here to alleviate this burden. The reduced order model is developed using data from the original high-fidelity finite element model (FEM). Static condensation is first used to obtain the stiffness matrix and linear equations of motion for the dynamic degrees of freedom. The restoring forces prescribed by the linear stiffness matrix are then substituted with hysteretic ones, calibrated by comparing the reduced order model time-history to the time-history of the initial FEM for a range of different excitations. This is posed as a least squares optimization problem and its efficient solution is facilitated through a sequential approach. The accuracy and the computational savings of the reduced order model are then examined for seismic risk assessment applications by comparing to the FEM predictions. A stochastic ground motion model is used to describe the seismic hazard and the accuracy for different levels of intensity is separately examined.

1. INTRODUCTION

Under strong seismic excitations, structural systems exhibit inelastic, hysteretic behavior and the evaluation of their dynamic response requires development of nonlinear finite element models (FEMs). For seismic risk/loss estimation (Haselton, et al. 2008) this is typically performed using either concentrated plasticity models, using nonlinear hinges to represent the behavior in locations of anticipated damages, or distributed inelasticity models, using a fiber discretization of the cross sectional area of all structural elements and adopting appropriate nonlinear constitutive laws for the material behavior. The computational burden of using such models in nonlinear response history analysis (NLRHA) is significant, especially for applications, like probabilistic d assessment, that require multiple NLRHAs.

Reduced order modeling offers an alternative modeling approach to alleviate this computational burden. Formally, reduced order models simplify the physics-based description of the original FEM through some form of condensation of the initial degrees of freedom and equations of motion (Jensen, et al. 2014). For facilitating the desired computational efficiency for seismic risk assessment applications, this condensation needs to be coupled with an approximation of the nonlinear (hysteretic) response characteristics. Retaining all nonlinearities associated with the hysteretic structural behavior offers little advantages in this setting. Parenthetically, should be pointed out that reduced order modeling is different from surrogate modeling, which offers a purely data-driven approximation of the structural response (Gidaris, et al. 2015), without invoking physics-based principles.

The calibration of the nonlinear properties of hysteretic reduced order models should be performed using data from the original nonlinear

FEM, with ultimate objective that the reduced order approximate model matches closely the high-fidelity one for excitations similar to the ones that is intended to be used for. Applications of reduced order modeling in earthquake engineering have been primarily constrained (Gidaris and Taflanidis 2013) to either calibration using real (recorded) data or to the direct use of the reduced order model, with no reference to an underlying nonlinear FEM. Though noteworthy attempts do exist for calibrating reduced order models by comparing to nonlinear FEMs (Gidaris and Taflanidis 2013, Tehrani, et al. 2018), they do have some limitations. Study by Gidaris and Taflanidis (2013) was constrained to shear-type of structural models and performed the reduced order model tuning using nonlinear static analysis. Study by Tehrani, et al. (2018) addressed any planar structural model and performed tuning using NLRHA, but was constrained to simple dynamic excitations for the tuning (quasi-static pushover, pulse and release, and pulse response), while it adopted a simplified parameterization of the nonlinear hysteretic force approximation and performed validation for limited excitations.

This study extends these efforts and establishes a comprehensive approach for tuning and validation of hysteretic reduced ordered models. Linear characteristics of the reduced order model are established using static condensation of the initial FEM, while nonlinear characteristics are calibrated by comparing response to the nonlinear FEM response under different earthquake acceleration time-histories. A sequential formulation of the associated least squares optimization problem (representing the calibration) is established so that approach can accommodate adoption of complex descriptions for the hysteretic forces for the reduced order model. Validation is performed with respect to seismic risk (seismic demand) estimation using a stochastic ground motion model to describe the seismic hazard (Vlachos, et al. 2018). Accuracy is separately examined for different levels of seismic intensity (different moment magnitude and rupture distance combinations).

2. REDUCED ORDER MODEL

2.1 Condensed structural model

In this study, emphasis is placed on planar structural models as shown in Figure 1. Under the common modeling assumptions of infinite axial floor rigidity and zero rotational mass for individual nodes, the model for the planar structure can be condensed to one degree of freedom per story (Chopra 2007). The corresponding stiffness matrix is obtained through static condensation of the original FEM. Modal truncation can be additionally utilized to further reduce the dynamic degrees of freedom considered, to correspond to displacements of specific floors instead of the displacements of all floors (Tehrani, et al. 2018). Here displacements of all floors are used.

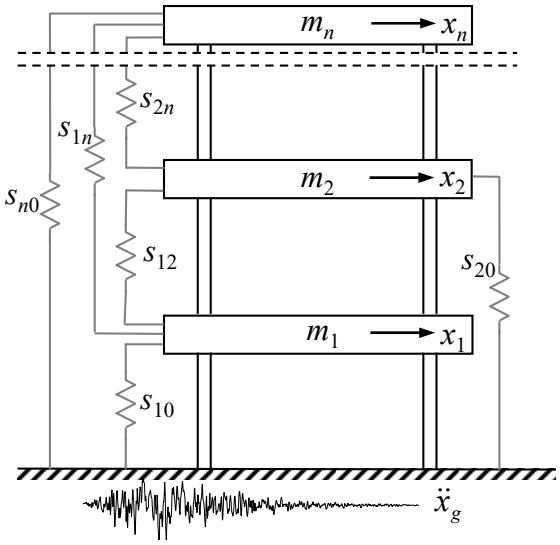

Figure 1:Structural model and representation through springs (in grey) connecting the different degrees of freedom

Let $\mathbf{x}_s \in \mathbb{R}^n$ denote the vector of displacements for each floor relative to the base (or, in general, of the displacements of the retained degrees of freedom). The equation of motion of the linear condensed model is:

$$\mathbf{M}_s\ddot{\mathbf{x}}_s + \mathbf{C}_s\dot{\mathbf{x}}_s + \mathbf{K}_s\mathbf{x}_s = -\mathbf{M}_s\mathbf{R}_s\ddot{x}_g \qquad (1)$$

where $\mathbf{M}_s$ and $\mathbf{K}_s$ are the $n \times n$ mass and stiffness matrices, respectively, both chosen to match the FEM ones, $\mathbf{C}_s$ is the $n \times n$ damping matrix,

modeled using the same assumptions as for the FEM (for example, Rayleigh damping as will be the case in the illustrative example later), $\mathbf{R}_s \in \mathbb{R}^n$ is the vector of earthquake influence coefficients (vector of ones) and $\ddot{x}_g \in \mathbb{R}$ represents the acceleration of the base. Equation (1) facilitates a match of the linear response between the reduced-order model and the high-fidelity FEM.

2.2 Representation through linear springs

Consider now the combination of all n_t=n(n-1) springs connecting the degrees of freedom to each other and to the ground, as also shown in Figure 1. The spring connecting degrees of freedom i and j is denoted by s_{ij} where i=1, …, n; j=0, i+1, …, n. Index j=0 is used to represent the connection to the ground. Let $\mathbf{T}_s$ be the $n_t \times n$ connectivity matrix relating the relative displacements at the ends of each spring δ_{ij} to vector $\mathbf{x}_s$. Each row of $\mathbf{T}_s$ corresponds to a separate spring s_{ij} and has all elements zero apart from the ith element equal to 1 and the jth element when $j \neq 0$ equal to -1. If $\boldsymbol{\delta}$ is the vector with relative spring displacements, δ_{ij}, then $\boldsymbol{\delta}$=$\mathbf{T}_s\mathbf{x}_s$. The condensed stiffness matrix can be equivalently expressed as:

$$\mathbf{K}_s = \mathbf{T}_s^T \mathbf{K}_l \mathbf{T}_s \tag{2}$$

where $\mathbf{K}_l$ is the diagonal matrix with elements k_{ij}^l defined as

$$\begin{aligned} k_{ij}^l &= [\mathbf{K}_s]_{ij} && \text{if } j \neq 0 \\ k_{i0}^l &= [\mathbf{K}_s]_{ii} - \sum_{k \neq i, k=1}^{n} [\mathbf{K}_s]_{ik} && \text{if } j = 0 \end{aligned} \tag{3}$$

where $[.]_{ij}$ represents the ijth element of a matrix. The spring formation in Figure 1 with spring characteristics k_{ij}^l given by Eq. (3) matches exactly the stiffness of the original linear FEM.

2.3 Hysteretic model

The formulation of the hysteretic reduced order model is established by modeling spring forces f_{ij} to be nonlinear instead of the linear ones $k_{ij}^l \delta_{ij}$. Each nonlinear spring force is defined as a function of the spring displacement δ_{ij} parameterized through n_t dimensional vector $\mathbf{q}_{ij}$. Typical choices for this function (Gidaris and Taflanidis 2013, Tehrani, et al. 2018) include piecewise linear elastic-perfectly plastic (PP) or peak-oriented (PO) models, generalized Masing models (GM) and Bouc-Wen (BW) models. When degradation is not considered, the parameters defining these hysteretic models are the following: PP and PO are defined through the yield displacement δ_{ij}^y and post-yield stiffness coefficient a_{ij}; GM requires, additionally, a parameter n_{ij} governing the smoothness of the transition from the linear to nonlinear range; BW requires, additionally, a parameter ρ_{ij} dictating the hysteretic loop shape. Therefore, n_t=2 for PP and PO, n_t=3 for GM and n_t=4 for BW. Modeling of degradation requires additional characteristics such as the displacement for the onset of deterioration and the coeficients for the strength/stiffness deterioration (Gidaris and Taflanidis 2013).

The hysteretic spring forces for all aforementioned models are given by

$$f_{ij} = a_{ij} k_{ij}^l \delta_{ij} + (1 - a_{ij}) g_{ij}(\delta_{ij}) \tag{4}$$

where the hysteretic function $g_{ij}(.)$ depends on the exact hysteretic model used and for small displacements δ_{ij} corresponds to a linear one, $k_{ij}^l \delta_{ij}$. For example, for the BW model which is the one preferred in the illustrative examples

$$g_{ij}(\delta_{ij}) = k_{ij}^l z_{ij} \tag{5}$$

with auxiliary variable z_{ij} obeying the first order differential equation

$$\dot{z}_{ij} = \dot{\delta}_{ij} - \frac{\rho_{ij}}{\left(\delta_{ij}^y\right)^{n_{ij}}} |\dot{\delta}_{ij}| |z_{ij}|^{n_{ij}-1} z_{ij} - \frac{1-\rho_{ij}}{\left(\delta_{ij}^y\right)^{n_{ij}}} \dot{\delta}_{ij} |z_{ij}|^{n_{ij}} \tag{6}$$

Details for the formulation of the other three hysteretic models can be found in Gidaris and Taflanidis (2013).

Not all spring s_{ij}, though, need to be necessarily modeled as hysteretic (i.e., inelastic) ones. Some can be considered as linear. We will use notation {.} to represent the combination of all springs (or their parameters) that are modeled

to be hysteretic. For example if only springs s_{12} and s_{23} are modeled as hysteretic, then $\{s_{ij}\}=[s_{12}\ s_{23}]^T$ and $\{k_{ij}^l\}=[k_{12}^l\ k_{23}^l]^T$. Size of $\{s_{ij}\}$, i.e. number of inelastic springs, is denoted n_c. The connectivity matrix for $\{s_{ij}\}$ is denoted by $\mathbf{T}_c$ and is obtained by retaining only the rows of $\mathbf{T}_s$ that correspond to elements of $\{s_{ij}\}$. The equation of motion of the hysteretic reduced order model are

$$\mathbf{M}_s\ddot{\mathbf{x}}_s+\mathbf{C}_s\dot{\mathbf{x}}_s+\mathbf{T}_c^T diag(\{g_{ij}(\delta_{ij})\})+\mathbf{K}_s^{rem}\mathbf{x}_s=-\mathbf{M}_s\mathbf{R}_s\ddot{x}_g \quad (7)$$

where *diag*(**a**) stands for diagonal matrix with diagonal elements corresponding to vector **a** and $\mathbf{K}_s^{rem}$ is matrix corresponding to linear spring components, given by

$$\mathbf{K}_s^{rem}=\mathbf{K}_s-\mathbf{T}_c^T diag(\{(1-a_{ij})k_{ij}^l\})\mathbf{T}_c \quad (8)$$

Structural model represented by Eq. (7) matches exactly the linear FEM response. The match to the nonlinear FEM response depends on how well the chosen hysteretic function approximates the actual hysteretic behavior and on the selection of parameters $\{\mathbf{q}_{ij}\}$ of that function. That selection is discussed next.

3. CALIBRATION OF INELASTIC PARAMETERS

3.1 Formulation of calibration problem

Calibration of the model parameters pertains to selection of $n_t n_c$ dimensional vector **q** corresponding to $\{q_{ij}\}$. This is established by comparing nonlinear time-history responses between the hysteretic reduced order model and the nonlinear FEM. Comparison should consider different earthquake excitations; since the objective of the reduced order model development is to replace the FEM for seismic demand (and loss) estimation, its calibration should consider same operational conditions, that is earthquake excitations, instead of simplified excitations.

To formalize this calibration let $[\ddot{x}_g^h\ ; h=1,..,n_h]$ represent the set of eartquakes considered and $\mathbf{y}=[y_l;\ l=1,\ldots,n_y]$ the set of response outputs used in the calibration. These outputs can include, for example, inter-storey drifts and absolute accelerations at different floors. Since seismic losses exhibit sifnigicant sensitivity to drift engineering demand parameters (Haselton, et al. 2008), and, furthermore, inelastic structural behavior typically results in residual drifts which play an important role in assessing structural performance, response output vector **y** should include at least inter-storey drifts, preferably for all floors. Also, for the *h*th earthquake calibration is performed over discretized time sequence $[t_r^h;\ r=1,\ldots,n_r^h]$, typically extending over the entire duration of the earthquake with some discretization interval *dt*. The output from NLRHA for the FEM for each earthquake and time instance will be denoted by $y_l^{FEM}(t_r^h\,|\,\ddot{x}_g^h)$. For the reduced order model corresponding notation will be $y_l^{RM}(t_r^h\,|\,\ddot{x}_g^h,\mathbf{p})$. The objective function is given by the weighted mean squared discrepancy between these response predictions

$$F(\mathbf{q})=\frac{1}{n_h}\sum_{h=1}^{n_h}\frac{1}{w_h}\left(\frac{1}{n_y}\sum_{l=1}^{n_y}\frac{1}{w_{hl}}\left[\frac{1}{n_r^h}\sum_{r=1}^{n_r^h}\frac{1}{w_{hlr}}e_{hlr}^2(\mathbf{p})\right]\right) \quad (9)$$

$$e_{hlr}(\mathbf{p})=(y_l^{FEM}(t_r^h\,|\,\ddot{x}_g^h)-y_l^{RM}(t_r^h\,|\,\ddot{x}_g^h,\mathbf{p}))$$

where w_h is the weight for each earthquake, w_{hl} is the weight for each output for the *k*th earthquake, w_{hlr} is the weight per time instance for *h*th output and *k*th earthquake, and e_{hlr} represents the discrepancy between the FEM and reduced order model time-histories.

Selection of **q** is finally posed as the nonlinear constrained optimization problem

$$\mathbf{q}^*=\underset{\mathbf{q}\in[\mathbf{q}_{\min},\mathbf{q}_{\max}]}{\arg\min}\ F(\mathbf{q})\quad \text{such that } \min(\text{eig}(\mathbf{K}_s^{rem}))>0 \quad (10)$$

where $[\mathbf{q}_{\min},\ \mathbf{q}_{\max}]$ represents the box-bounded constraint for **q** and $\min(\text{eig}(\mathbf{K}_s^{rem}))$ corresponds to the minimum eigenvalue for matrix $\mathbf{K}_s^{rem}$. The constraint for that eigenvalue being positive guarantees that the reduced order model corresponds to a stable structural model. This constraint is introduced to guarantee bounded objective function $F(\mathbf{q})$.

3.2 Sequential optimization

Optimization problem of Eq. (10) is nonconvex and has a costly objective function involving n_h

NLRHAs for the reduced order model. Solution of this optimization is performed here through two step approach, combining an efficient global optimization (EGO) first step (Jones, et al. 1998) to search the entire [$\mathbf{q}_{\min}$, $\mathbf{q}_{\max}$] domain and identify a candidate global optimum and a gradient-based optimization (NPSOL) second step (Gill, et al. 1986) to further locally improve upon this solution.

For problems with large dimensional vector $\mathbf{q}$ the cost associated with the global search over domain [$\mathbf{q}_{\min}$, $\mathbf{q}_{\max}$] can be prohibitively high. Since that global search is important due to the non-convex nature of the problem a sequential optimization is proposed here. The basic idea is to gradually and hierarchically increase the number of springs that are considered as inelastic, starting from the most important ones, and at each iteration optimize only for the newly added spring parameters. Importance of springs is evaluated by distance $|i\text{-}j|$ since it is well understood that stiffness-interaction between stories decreases as these stories are further apart. The optimization workflow is set as follows

Initialization: select the maximum order for springs considered potentially as inelastic n_{max}. Consider first as inelastic springs $\{s_{ij}\}$ with $|i\text{-}j|=1$, that is inter-storey springs, and optimize for their parameters $\{q_{ij}\}$ through optimization of Eq. (10) using first a global (EGO) step and then a local (NPSOL) optimization step. Set spring order $q=2$.

Iteration q: Consider as inelastic the springs $\{s_{ij}\}$ for which $|i-j|\le q$. Optimize only for parameters $\{q_{ij}\}$ of springs for which $|i\text{-}j|=q$, setting inelastic parameters for springs for which $|i\text{-}j|<q$ equal to the parameters identified in previous iterations. Identify new spring inelastic parameters through optimization of Eq. (10) using first a global (EGO) step and then a local (NPSOL) optimization step. Any spring for which optimal a_{ij} is identified to be equal to 1, is considered as linear for all subsequent iterations. Set spring order $q=q+1$ and proceed to next iteration if $q+1\le n_{\max}$, else perform final optimization.

Final optimization: Now simultaneously optimize for all $\{s_{ij}\}$ with $|i-j|\le n_{\max}$ through optimization of Eq. (10) using local optimization (NPSOL) with starting point the solution that has been identified in the previous iterations.

Final optimization stage establishes a simultaneous gradient-based optimization of all nonlinear spring parameters, with initial point the values identified through the global optimization sub-problems in the previous iterations. The hierarchical addition of inelastic springs reduces dimensionality of the problem (at most $n_t n$ parameters per iteration), facilitating efficient global search. This hierarchical addition ignores, though, correlations between spring of different order (springs $|i\text{-}j|<q$ and springs $|i=j|=q$ are independently optimized), which is the reason the final optimization stage is included, explicitly considering simultaneous optimization for all springs. The maximum order $n_{\max}$ is introduced to reduce computational burden for problems with large number of floors. The underlying assumption is, here, that consideration as inelastic springs greater than $n_{\max}$ floors apart will have negligible impact on the nonlinear behavior and on the objective function $F(\mathbf{q})$.

3.3 Selection of type of hysteresis

For selecting the type of hysteresis all possible models should be considered, for example PO, PP, GM and BW discussed earlier, and the one corresponding to the smaller objective function value $F(\mathbf{q}^*)$ should be adopted. Model parsimony can be incorporated in the analysis, if desired, using Bayesian inference, for example the well-known Bayesian information criterion.

3.4 Selection of earthquake excitations

The selection of the earthquake excitation set [$\ddot{x}_g^h$; $h=1,..,n_h$] is critical for the proper calibration of the spring inelastic parameters. This set should excite all essential components of the FEM nonlinear behavior, providing sufficient information for the calibraiton of the corresponding nonlinear reduced order model springs. This can be accomplished if a large number of excitations is examined. These do not

need to be distinct, rather scaling of the same earthquakes can be also considered, for example inclusion of both $\ddot{x}_g^h$ and $1.5\ddot{x}_g^h$. The range of excitation intensities should encompass the operating conditions that the reduced order model will be used for. For example, if reduced order model is intended to be used for excitations resulting in significant degree of nonlinear behavior, then calibration should not be constrained to excitations producing moderate only degree of nonlinear behavior.

4. ILLUSTATIVE EXAMPLE

For the illustrative example the three story benchmark steel structure described in (Ohtori, et al. 2004) is used. Plan dimensions are 36.58 m by 54.87 with total height of 11.89m. The building's lateral load load-resisting system is comprised of moment resisting frames(MRFs) and analysis is performed along the short dimension. The nonlinear FEM model of this building is created OpenSees (McKenna 2011). Fiber modeling is adopted with material characteristics: 1) modulus of elasticity E=1.99 10^5 Mpa for both beams and columns, 2) yield stress for the columns 345 MPa and for the beams 248 MPa and 3) use of the Giuffre'-Menegotto-Pinto model for the steel fibers with isotropic strain hardening, with all the parameters having the default values (Filippou, et al. 1983) and the strain-hardening ratio being 0.02 for both beam and columns. Damping matrix C_s is modeled through Rayleigh damping assumption with damping ration selected as 2% for 1st and 3rd modes. The reduced order models are developed in SIMULINK simulation environment using guidelines discussed in study by Gidaris and Taflanidis (2013) for performing the NLRHA. For a time-step of 0.01 and using Newmark's average acceleration for numerical integration and for excitation of duration 40 s (this corresponds to Loma Prieta excitation using later in validation) the computational time required for the NLRHA in a desktop with 4core Xeon 3.1GB processor is 72s for the OpenSees model and 0.9s for the reduced order model, demonstrating the significant computational savings the latter offers providing in this case almost two orders of magnitude reduction for computational effort (80 fold reduction).

4.1 Model calibration

For the calibration three different excitations are considered: Kobe, Northridge and Friuli. Three different calibration scenarios are examined. First one, termed SC_1, used the three different excitations (n_h=3), second, termed SC_2, considers additionally scaled excitations using scaling 1.25 (n_h=6), third, termed SC_3, considers additionally scaled excitations with scaling 1.5. So the three scenarios are progressively enhanced with higher intensity excitations. The reduced order models calibrated through each of the considered scenarios are denoted, respectively by D_1, D_2 and D_3. For each earthquake the strong ground motion duration with discretization dt=0.01 is assumed for defining t_r. Weights are chosen w_h=w_{lhr}=1 (equal importance for all earthquakes and time instances) and

$$w_{hl} = \frac{1}{n_r^h}\sum_{r=1}^{n_r^h}(y_l^{FEM}(t_r^h \mid \ddot{x}_g^h))^2 \qquad (11)$$

establishing a normalization for each output with respect to its variance for each earthquake.

Three different hysteretic models are examined, PP, GM and BW and results are reported in Table 1. It is evident that BW clearly outperforms the other ones and is the one considered for the remainder of the discussions. Table 2 presents the objective function value $F(\mathbf{q})$ evaluated for the three different designs D_1, D_2 and D_3 for each calibration scenario. Results show that performance is similar across all different calibrations, especially for SC_2 and SC_3, indicating that even the initial selection of the three earthquakes has sufficient information to identify all spring nonlinearities.

Table 1: Optimal value of objective function $F(\mathbf{q}^*)$ for different hysteretic models and calibration scenarios

Hysteretic model	Calibration scenario		
	SC_1	SC_2	SC_3
PP	0.0927	0.1119	0.1181
GM	0.0521	0.0492	0.0770
BW	0.0220	0.0238	0.0269

Table 2: Value for $F(\mathbf{q})$ for the three different calibration scenarios for the three different calibrated designs for BW model

	Calibration scenario		
	SC_1	SC_2	SC_3
D_1	0.0220	0.0266	0.0304
D_2	0.0379	0.0238	0.0279
D_3	0.0667	0.0305	0.0269

4.2 Validation

Validation is first examined looking at time-history response. Figure 2 presents comparison of time-histories between OpenSees and BW D_3 reduced order model for top floor drift and acceleration for Loma Prieta earthquake. Very good agreement is reported across the entire time-history, extending to both peak and residual responses.

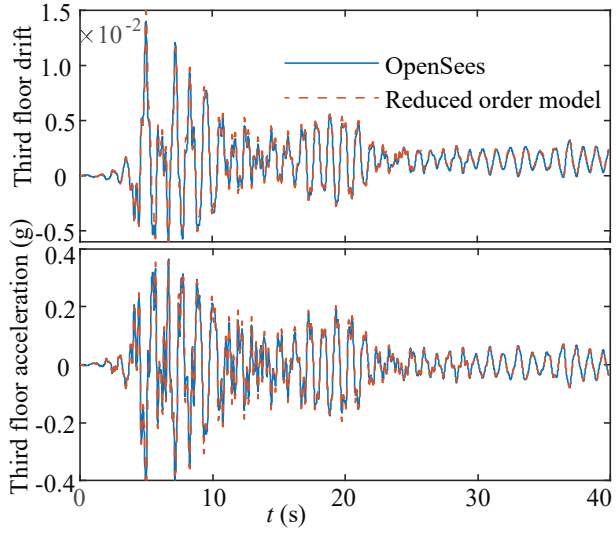

Figure 2: Validation of reduced order model through time-history comparison of drift and acceleration outputs to OpenSees FEM for Loma Prieta earthquake

A more interesting comparison is, of course, with respect to risk estimation, instead of individual excitations. For describing the seismic hazard for this comparison the stochastic ground motion model developed recently by Vlachos et al. (2018) is used. Four different seismicity scenarios are considered corresponding to combinations of moment magnitude M=[6.5, 7.5] and rupture distance R=[20, 50] km. With respect to local site conditions (required by ground motion model) the shear wave velocity at top 30 m of soil 600 m/s. Seismic risk is expressed with respect to the probability that some engineering demand parameter *EDP* will exceed specific threshold β, $P[EDP>\beta]$ for a range of thresholds. Total of 500 ground motions are used for each seismicity scenario to describe the seismic hazard. Results are reported for *EDP* inter-story drift in Figures 3 and 4, though results for acceleration show similar trends. Figure 3 shows comparison for calibration D_3 for different inter-storey drifts and Figure 4 shows comparisons for selective seismicity scenarios for all calibration cases.

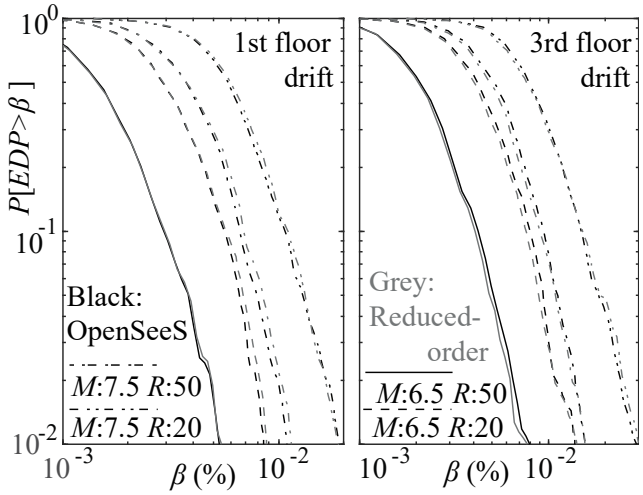

Figure 3: Validation of reduced order model D_3 in seismic risk estimation setting for all examined seismicity scenarios.

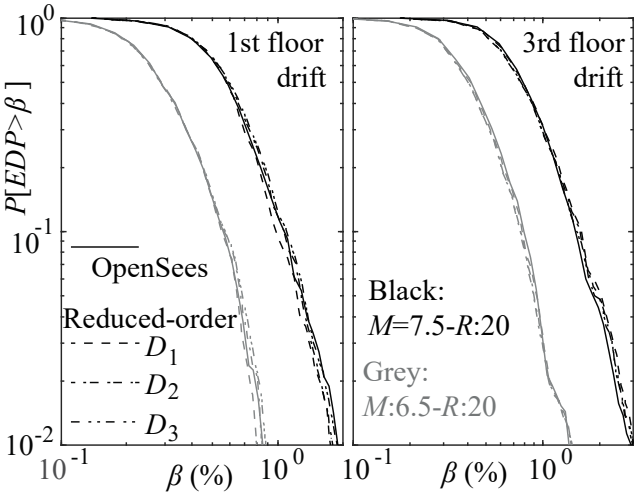

Figure 4: Validation of all reduced order model calibrations D_1-D_3 in seismic risk estimation setting for selective seismicity scenarios.

Results show that the proposed calibration approach facilitates very good agreement with respect to risk estimates for all cases. When considering the substantial computational savings provided through the reduced order model, these comparisons demonstrate the benefits that the proposed calibration framework can provide for seismic loss assessment applications.

5. CONCLUSIONS

The calibration of reduced order hysteretic structural models and subsequent validation in seismic demand estimation setting was examined in this paper. Calibration was established by comparing nonlinear time-histories to the initial structural FEM, and a sequential optimization was established to accommodate the adoption of complex descriptions for the reduced order model hysteretic forces. Validation within the illustrative example demonstrated the substantial computational savings and high accuracy risk estimation that can be achieved through the proposed framework.

6. ACKNOWLEDGMENTS

Authors would like to thank Dr. Papakonstantinou for prodiving the codes for generation of synthetic acceleration time-histories using the (Vlachos, et al. 2018) model.

7. REFERENCES

C. B. Haselton, C. A. Goulet, J. Mitrani-Reiser , and J. L. Beck, "An assessment to Benchmark the seismic performance of a code-conforming reinforced concrete moment-frame building," PEER 2008.

H. Jensen, E. Millas, D. Kusanovic, and C. Papadimitriou, "Model-reduction techniques for Bayesian finite element model updating using dynamic response data," *Computer Methods in Applied Mechanics and Engineering,* vol. 279, pp. 301-324, 2014.

I. Gidaris, A. A. Taflanidis, and G. P. Mavroeidis, "Kriging metamodeling in seismic risk assessment based on stochastic ground motion models," *Earthquake Engineering & Structural Dynamics,* vol. 44, pp. 2377–2399, 2015.

I. Gidaris and A. A. Taflanidis, "Parsimonious modeling of hysteretic structural response in earthquake engineering: Calibration/validation and implementation in probabilistic risk assessment," *Engineering Structures,* vol. 49, pp. 1017-1033, 2013.

M. Tehrani, P. Harvey Jr, H. Gavin, and A. Mirza, "Inelastic condensed dynamic models for estimating seismic demands for buildings," *Engineering Structures,* vol. 177, pp. 616-629, 2018.

C. Vlachos, K. G. Papakonstantinou, and G. Deodatis, "Predictive model for site specific simulation of ground motions based on earthquake scenarios," *Earthquake Engineering & Structural Dynamics,* vol. 47, pp. 195-218, 2018.

A. K. Chopra, *Dynamics of structures: theory and applications to earthquake engineering*, vol. 3: Pearson/Prentice Hall Upper Saddle River, NJ, 2007.

D. Jones, M. Schonlau, and W. Welch, "Efficient global optimization of expensive black-box functions," *Journal of Global optimization,* vol. 13, pp. 455-492, 1998.

P. E. Gill, W. Murray, M. A. Saunders, and M. H. Wright, "User's guide for NPSOL (version 4.0): A Fortran package for nonlinear programming," Stanford Univ CA Systems Optimization Lab 1986.

Y. Ohtori, R. Christenson, B. Spencer Jr, and S. Dyke, "Benchmark control problems for seismically excited nonlinear buildings," *Journal of Engineering Mechanics,* vol. 130, pp. 366-385, 2004.

F. McKenna, "OpenSees: A framework for earthquake engineering simulation," *Computing in Science and Engineering,* vol. 13, pp. 58-66, 2011.

F. C. Filippou, V. V. Bertero, and E. P. Popov, "Effects of bond deterioration on hysteretic behavior of reinforced concrete joints," 1983.